LuxTag: Ambient Light Sensing and Localization via Passive RFID

Xingyu Chen
State Key Laboratory for Novel Software Technology
Nanjing University
Nanjing, China

Jia Liu*
State Key Laboratory for Novel Software Technology
Nanjing University
Nanjing, China

Chengxuan Fu
State Key Laboratory for Novel Software Technology
Nanjing University
Nanjing, China

Lei Xie
State Key Laboratory for Novel Software Technology
Nanjing University
Nanjing, China

Yanchao Zhao
Nanjing University of Aeronautics and Astronautics
Nanjing, China

Baoliu Ye
State Key Laboratory for Novel Software Technology
Nanjing University
Nanjing, China

Chen Tian
State Key Laboratory for Novel Software Technology
Nanjing University
Nanjing, China

Guihai Chen
State Key Laboratory for Novel Software Technology
Nanjing University
Nanjing, China

Abstract

RFID has revolutionized item-level intelligence in IoT ecosystems, yet static localization with passive tags remains challenging due to multipath interference inherent in RF signals. We present LuxTag, the first system to enable visible light-based sensing and localization using standard, commercial RFID tags by transforming them into ambient light sensors. Our key insight leverages the discovery that photon-induced leakage currents in passive RFID ICs modulate their persistence time (i.e., the duration a tag remains operational after RF excitation ceases) proportional to ambient illuminance. LuxTag introduces two innovations: (i) a first-principles model characterizing how ambient light alters tag persistence time, enabling battery-free light sensing without hardware modifications; (ii) a differential measurement technique and zero-shot calibration method to isolate light effects and autonomously derive tag parameters, ensuring robust and accurate static localization system using COTS RFID infrastructure. Extensive experiments demonstrate that LuxTag achieves a mean light intensity error of 3.6 lux and 60.7% improvement over state-of-the-art static RFID localization. By synergizing the ubiquity of RFID with the multipath resilience of optical sensing, LuxTag opens new avenues for static RFID localization in smart warehouses, retails, and beyond.

CCS Concepts

• **Networks** → **Sensor networks**; **Location based services**.

*Corresponding author (jialiu@nju.edu.cn).

SenSys '26, Saint Malo, France

ACM ISBN 979-8-4007-2309-4/26/05
https://doi.org/10.1145/3774906.3802778

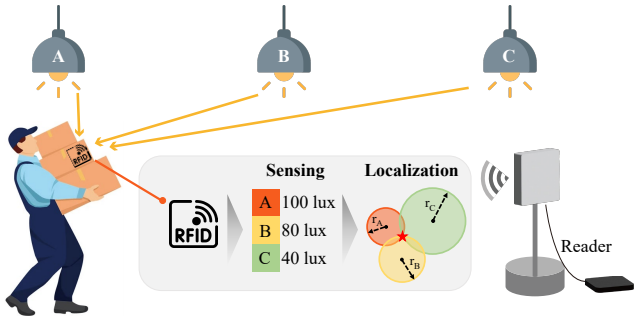

Figure 1: Overview of LuxTag: Enabling a passive, standard COTS RFID tag to do ambient light sensing and localization.

Keywords

RFID, static RFID localization, ambient light sensors, ambient light localization

ACM Reference Format:
Xingyu Chen, Jia Liu, Chengxuan Fu, Lei Xie, Yanchao Zhao, Baoliu Ye, Chen Tian, and Guihai Chen. 2026. LuxTag: Ambient Light Sensing and Localization via Passive RFID. In *ACM/IEEE International Conference on Embedded Artificial Intelligence and Sensing Systems (SenSys '26), May 11–14, 2026, Saint Malo, France.* ACM, New York, NY, USA, 13 pages. https://doi.org/10.1145/3774906.3802778

1 Introduction

Radio Frequency Identification (RFID) has emerged as a pivotal technology for pervasive item-level intelligence in IoT ecosystems. The deployment of battery-free passive tags (<$0.02/unit) enables cost-effective digitalization of physical objects across supply chains [21, 25, 37], access control systems [9, 33], and smart environments [19, 30, 31]. Beyond mere identification, the potential for RFID systems to provide precise localization has spurred

significant research interest [14, 16, 22, 28, 34]. Accurate, low-cost item tracking within complex environments like warehouses, retail spaces, or smart factories remains a critical challenge, driving the development of RFID-based localization techniques.

Applications that require high-accuracy RFID localization, especially *static RFID localization* – where both tags and infrastructure (reader) remain fixed – are abundant across industries. For example, in modern warehouses, static RFID localization can improve the accuracy and speed of inventory tracking by providing real-time, precise location data for each item. This allows for automatic updates to inventory levels, reducing human error, improving efficiency, and enhancing supply chain visibility. In retail environments, accurate in-store product localization can aid in stock management, improve customer experience through fast checkout and personalized services, and streamline replenishment workflows. Additionally, static RFID localization enables precise tracking of inventory in real-time, reducing stockouts and theft. In libraries, static RFID localization can help automate shelf management, reduce misplaced books, and assist with inventory audits, ensuring that books are accurately located and easy to find.

Existing RFID localization primarily leverages RF signal properties such as Received Signal Strength Indicator (RSSI) [14, 22], phase difference [16, 28, 34], or Doppler shift [2, 24]. While these methods have achieved notable progress, they fundamentally struggle with multipath effects – an enduring problem in RF systems [8, 18, 27]. These multipath effects arise from the specular (mirror-like) reflection behavior of RF waves, where wavelengths (e.g., $\lambda \approx 0.3$ m for UHF RFID) are often significantly larger than the average surface roughness at common environmental boundaries like walls or shelving units (~0.1 mm). Consequently, signals reflect coherently, leading to complex superposition at the receiver that is exceptionally difficult to model or disentangles.

To address these issues, recent efforts have employed Synthetic Aperture Radar (SAR) and differential techniques [4, 26, 29, 34], enhancing spatial resolution and multipath resilience through controlled reader or tag movement to synthesize virtual antenna arrays. While these approaches have advanced mobile RFID localization, *static RFID localization – where both tags and infrastructure (reader) remain fixed* – continues to be an open problem in real-world deployments. The primary issue lies in the persistent impact of multipath signals, which are difficult to isolate or eliminate without dynamic spatial sampling. Although state-of-the-art Time-of-Flight (ToF) methods [7, 17] attempt to address multipath by extracting direct-path signals, they suffer from narrow-band (about 20 MHz) RFID systems, which are insufficient for fine-grained applications demanding higher localization accuracy. Thus, improving localization accuracy and reducing the impact of multipath effects in static RFID settings is crucial for advancing the practical deployment of RFID-based systems in complex, dense environments.

To overcome the fundamental limitations of static RF-based localization, this paper introduces LuxTag, a novel approach enabling ambient light sensing and localization using passive, standard RFID tags. Unlike RF signals, optical signals in the visible spectrum (wavelength $\lambda = 400 \sim 750$ nm) interact with surfaces predominantly through *diffuse reflection* due to their significantly shorter wavelength. This diffuse scattering inherently suppresses coherent interference and multipath effects, offering a more robust foundation for spatial sensing [10, 36, 39]. LuxTag uniquely bridges two domains: It leverages the established infrastructure and deployment advantages of ubiquitous RFID systems – including battery-free tags, standardized readers, and existing RF backscatter communication – while exploiting the inherent multipath resilience offered by diffuse light propagation. However, harnessing this advantage requires measuring light intensity at the tag's location – a capability absent in standard RFID tags.

Bridging this gap, LuxTag establishes a physical-layer cross-modality by transforming commercial off-the-shelf (COTS) passive RFID tags into ambient light sensors, leveraging the sensed light intensity to determine tag locations. As illustrated in Fig. 1, multiple light sources (e.g., ceiling incandescent bulbs A, B, and C) illuminate the environment. The RFID reader communicates with passive tags, measures the light intensity incident on the tag surface, and estimates the tag-to-light-source distances to enable trilateration-based localization. LuxTag addresses two long-standing challenges: (1) exploring a light-intensity-dependent metric that can be accessed through the RF interface, and (2) designing a standard-compliant measurement approach that remains robust under varying environmental conditions.

The core insight of LuxTag stems from the discovery that *photon-induced leakage currents within the tag's integrated circuit (IC) accelerate the discharge rate of its internal storage capacitor.* Critically, this discharge rate – and thus the tag's intrinsic persistence time (i.e., the duration it sustains operation and backscattering capability after the reader's RF signal ceases) – varies inversely with the ambient illuminance level. LuxTag precisely formulates the relationship between persistence time and illuminance. To ensure robustness against environmental factors (i.e., temperature, tag diversity), LuxTag introduces a differential measurement technique coupled with a zero-shot calibration method, concurrently enabling robust light sensing and static tag localization without manual per-tag calibration. We implement a prototype of LuxTag with COTS RFID. Extensive experimental evaluation demonstrates that LuxTag achieves high-precision static localization, in comparison to existing RF-based methods. In summary, by synergizing the ubiquity of RFID with the multipath resilience of optical sensing, LuxTag introduces a new paradigm for robust and accurate static RFID localization. The main contributions of this work are threefold.

- We present LuxTag, the first system to transform standard, commercial RFID tags into optical sensors for accurate ambient light sensing and localization, bridging the multipath resilience of light with the ubiquity of RF infrastructure.
- We build the theoretical and experimental model of how ambient light modulates a tag's persistence time and introduce a zero-shot calibration method that concurrently enables robust light sensing and tag localization without manual per-tag calibration.
- We implement LuxTag using COTS RFID. Extensive experimental evaluation demonstrates that LuxTag achieves mean light intensity errors of 3.6 lux, and mean localization errors of 22.5 cm, outperforming the state-of-the-art.

2 Overview

In this section, we analyze the fundamental limitations of RF-based localization and demonstrate the distinct advantages of optical localization, establishing the core principles underlying our design.

2.1 Multipath in RF-Based Localization

Existing RFID localization methods rely on RF signal properties such as Received Signal Strength Indicator (RSSI) [14, 22], phase difference [16, 28, 34], or Doppler shift [2, 24]. While these techniques achieve meter- to decimeter-level accuracy in controlled settings, they fundamentally suffer from multipath interference. These limitations stem from the specular (mirror-like) reflection behavior of RF waves (e.g., UHF RFID's $\lambda \approx 0.3$ m), where common building materials like drywall (surface roughness $h \approx 0.1$ mm), concrete ($h \approx 1$ mm), and metal surfaces ($h \approx 0.01$ mm) all satisfy the Rayleigh criterion for mirror-like reflection ($h < \frac{\lambda}{8cos\theta}$) [38], where θ is the incident angle. This results in coherent reflections that create complex signal superposition at the receiver, introducing unpredictable errors – especially in cluttered environments like warehouses or smart factories [27].

To address these issues, recent efforts have employed Synthetic Aperture Radar (SAR) and differential techniques [4, 26, 29, 34], enhancing spatial resolution and multipath resilience through controlled reader movement to synthesize virtual antenna arrays. While these approaches have advanced mobile RFID localization, *static tag localization* – where both tags and infrastructure (reader) remain fixed – still remains an open problem in real-world deployments. The primary issue lies in the persistent impact of multipath signals, which are exceedingly difficult to isolate or eliminate without dynamic spatial sampling. Although state-of-the-art Time-of-Flight (ToF) methods [7, 17] attempt to address multipath by extracting direct-path signals, they achieve only a median localization error of ~57 cm in narrow-band RFID systems, which are insufficient for fine-grained applications demanding higher localization accuracy. These limitations stem from fundamental physics rather than implementation details – as long as localization relies on RF signals with wavelengths much larger than surface roughness, multipath will remain an insurmountable challenge, especially for static

2.2 Optical Spectrum

The optical spectrum offers a fundamentally different propagation paradigm that inherently avoids the multipath challenges of RF-based systems. Visible light wavelengths ($\lambda = 400 \sim 750$ nm) are approximately six orders of magnitude smaller than UHF RFID signals, changing the fundamental interaction with surfaces. At these scales, even smooth-appearing materials like painted drywall ($h \approx 0.1$ mm) present surface roughness hundreds of times larger than the wavelength, satisfying the condition for diffuse reflection where incident light is scattered in all directions rather than reflected coherently. This diffuse scattering behavior has three key advantages for localization: First, it eliminates the standing wave patterns and fading effects caused by coherent interference; second, it makes received light intensity primarily dependent on LOS distance from the source following the inverse square law ($I \propto 1/r^2$) rather than being dominated by reflection paths; third, it enables

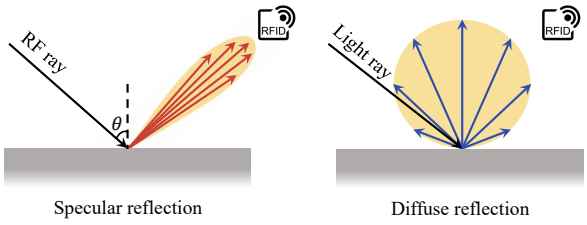

Figure 2: Specular reflection vs. diffuse reflection.

simple geometric models for light propagation that remain accurate even in complex environments.

We quantitatively validate the multipath characteristics of RF versus optical signals under the same laboratory conditions. Theoretical values (benchmarked at 1 meter) are provided according to the inverse-square law. As shown in Fig. 3, the measured values of the optical signal closely match the theoretical values as distance increases. At a distance of 1 meter, the light intensity is 125 lux. At 2 meters, the measured intensity reduces to 34.58 lux, deviating from the theoretical value ($125/4 = 31.25$ lux) by only 3.33 lux. At 3 meters, the measured intensity is 14.8 lux, differing from the theoretical value ($125/9 = 13.89$ lux) by only 0.91 lux. In contrast, the RSSI values of the RF signal exhibits significant errors at 2 meters and 2.5 meters. Theoretically, the RSSI at 2.5 meters should have decreased by 3.88 dB compared to that at 2 meters, but the actual measurement shows an increase of 6.6 dB due to multipath effects, resulting in an error of 10.48 dB (nearly a tenfold difference). The experimental results well indicate that optical localization is less affected by multipath interference than RF-based localization.

Furthermore, visible light's inability to penetrate most materials (attenuation > 20 dB/cm for walls) naturally confines localization to line-of-sight scenarios where accuracy is highest, unlike RF signals that propagate through obstacles but with unpredictable distortions. The combination of these properties makes light an ideal medium for precise localization. However, harnessing this advantage for localization requires measuring light intensity at the tag's location – a capability absent in standard RFID tags. Bridging this gap, enabling a physical-layer cross modality where an RF communication device performs optical sensing for localization, presents a significant and underinvestigated challenge.

3 Design of LuxTag

In this section, we convert billions of deployed passive RFID tags into light sensors, requiring no hardware changes to existing RFID infrastructure (readers, antennas, and tags).

3.1 New Optical Metric: Persistence Time

LuxTag's innovation lies in transforming standard passive RFID tags into optical sensors by exploiting their persistence time – the duration a tag remains operational after the RF excitation field is removed. This persistence time [1], typically being a few seconds for EPC Gen2 tags, is determined by the discharge rate of the tag's internal storage capacitor that powers the IC between RF bursts.

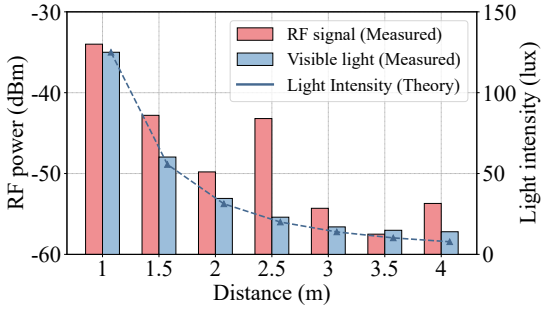

Figure 3: Different propagation characteristics.

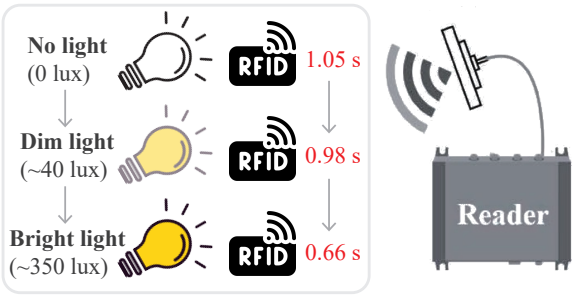

Figure 4: Persistence time vs. light intensity.

More specifically, passive RFID tags operate without an internal power source, instead harvesting energy from the electromagnetic RF signals emitted by the reader. Structurally, each tag comprises two key components: (1) A carefully designed antenna optimized for UHF frequencies, and (2) a microchip containing the tag's logic circuitry and memory. The microchip is directly connected to the antenna terminals, forming an integrated system where incident RF energy is converted to operational power through electromagnetic induction. When the tag enters the reader's RF field, the antenna captures electromagnetic energy, inducing an alternating voltage across its terminals. This voltage powers the tag's operations through a process analogous to an RC (resistor-capacitor) charging circuit. If RF power is interrupted, the system transitions to a discharging mode. This discharge current maintains the chip's operation temporarily: a phenomenon we term the persistence time – a property LuxTag exploits for ambient light sensing.

We discovered that ambient light induces measurable changes in this persistence time through photon-generated leakage currents in the tag's CMOS circuitry. When photons with energy exceeding the silicon bandgap strike the IC, they generate electron-hole pairs that create additional discharge paths across reverse-biased junctions. This photon-induced leakage current accelerates the capacitor discharge, resulting a reduction of the persistence time as the light intensity increases. Fig. 4 plots the relationship between the persistence time and the light intensity, where the persistence time is measured through SQM [6] with a COTS RFID reader. As we can see, when light intensity increases from 0 to ~350 lux, the persistence time drops from 1.05 s to 0.66 s. The general trend accords with our expectation, which validates the feasibility of optical sensing. This discovery effectively converts billions of deployed passive RFID tags into light sensors, requiring no hardware changes to existing infrastructure.

Translating the light-persistence effect into a practical light sensing and localization system presents two major challenges. (1) Lack accurate modeling of nonlinear relationship between persistence time and illuminance. LuxTag combines empirical characterization of tag-specific parameters with physical modeling of the leakage current mechanisms, achieving accurate illuminance estimation. (2) Environmental factors like temperature and tag diversity introduce significant measurement noise [5, 6]. The need for per-tag calibration would normally prevent large-scale deployment. LuxTag presents a zero-shot calibration method that solves this by leveraging differential measurement and invariant intensity ratios of multiple light sources, regardless of the temperature varies and the tag diversity.

3.2 Modeling Persistence Time and Light Intensity

RFID tags utilize numerous electronic components within their circuitry, including the widespread use of capacitors, inductors, diodes, and transistors. These components enable the tags to manage energy and execute complex logical operations. If light affects the internal components within an RFID tag, it could influence the associate tag function and be observed through an RFID reader. The persistence time is just a function that we want. Specifically, Fig. 5 shows a typical circuit that can enable persistence of a tag. When the reader charges the circuit, it applies a voltage (V_{in}), charging a target capacitor. When charging stops, the capacitor starts discharging through the tag circuit, creating a discharge current (I_s). If the voltage across this capacitor drops below the tag's minimum operating voltage (V_0), the tag will lose function, causing what we called persistence time.

To prevent stored charge from leaking back into the charging path during discharge, the circuit employs a diode. This diode can significantly reduce unwanted reverse current (I_k), effectively blocking it and protecting the intended discharge time. In dark environment (without light), I_k is very small. This is because the diode's internal 'depletion region' acts like a barrier, lacking the free charge carriers (electrons and holes) needed to easily conduct current in reverse. However, when light hits the diode, photons provide energy that generates new pairs of free electrons and holes (electron-hole pairs). As a result, I_k flows much more easily. The capacitor voltage drops faster toward the threshold V_0. This faster discharge means a shorter persistence time.

According to the circuit shown in Fig. 5, we can establish the relationship between persistence T and light intensity:

$$T = \frac{C\Delta V}{I_s + I_k}, \tag{1}$$

where C denotes capacitance, $\Delta V = V_{in} - V_0$ is the voltage drop from initial charge to minimum operating voltage V_0, I_s is the designed

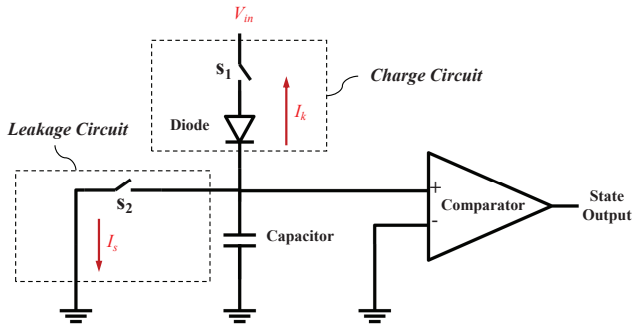

Figure 5: The persistence circuit of a tag.

discharge current, and I_k represents the light-sensitive reverse current of the blocking diode. I_k can be further decomposed into two components:

$$I_k = I_{dark} + I_{light}, \tag{2}$$

where I_{dark} is the baseline dark current, while $I_{light} = \kappa P_{\text{light}}$ is the light-induced current proportional to light intensity P_{light} with coefficient κ. Substituting into Eq. (1) yields:

$$T = \frac{C\Delta V}{I_s + I_{dark} + \kappa P_{\text{light}}} = \frac{1}{\alpha P_{\text{light}} + \beta}, \tag{3}$$

where $\alpha = \frac{\kappa}{C\Delta V}$ and $\beta = \frac{I_s + I_{dark}}{C\Delta V}$. Without environment variations, α and β are constants determined by the tag's hardware structure. This confirms a linear relationship between T's inverse and light intensity, which can be written as:

$$\frac{1}{T} = \alpha P_{\text{light}} + \beta. \tag{4}$$

To validate the derived relationship between persistence time (T) and illuminance (P_{light}), we conduct controlled experiments where a COTS RFID tag is exposed to varying light intensities. The illuminance is systematically adjusted by positioning the tag at different distances from a calibrated 200 W LED bulb, while an industrial-grade illuminance meter records ground-truth P_{light} values. For each position, we measure the tag's persistence time T through precise RF power cycling at the reader. As shown in Fig. 6, the inverse persistence time ($\frac{1}{T}$) exhibits a strong linear correlation with measured P_{light} across the tested range, confirming our theoretical model.

3.3 Light Sensing

In theory, determining the parameters α and β requires two distinct measurements of persistence time under different light intensities P_{light1} and P_{light2}:

$$\begin{cases} \frac{1}{T_1} = \alpha P_{\text{light1}} + \beta, \\ \frac{1}{T_2} = \alpha P_{\text{light2}} + \beta. \end{cases} \tag{5}$$

Solving this system of equations yields the values of α and β. While straightforward in principle, both α and β are highly sensitive to temperatures and tag diversity, which lowers the sensing accuracy. We conducted experiments to quantify these effects, measuring α and β for ten tags under identical system setups while varying temperature. As shown in Fig. 7, both parameters of the same tag exhibit significant variation with temperature changes. For instance, α decreases by approximately 19.5% and β increases by 12.8% as temperature rises from 10°C to 40°C. Moreover, Fig. 8 shows tag diversity introduces additional variability: under the same temperature and light conditions, α and β values of 5 tags vary largely due to manufacturing tolerances in components such as capacitors and diodes. This dual dependency necessitates separate calibration for each tag at multiple temperatures, forming a pre-calibrated lookup tables for later use.

However, we do not know the environmental temperature in practical use. To address this problem, we develop a dual-tag calibration approach, utilizing one shielded RFID tag (covered by light-resistance material such as black tape) as a temperature sensor to measure ambient temperature, and then applying the temperature-corresponding parameters to calibrate another tag for accurate light intensity measurement. In our method, the temperature sensor is itself a standard RFID tag, which employs the Thermotag [6] for reliable temperature monitoring. Using an RFID tag rather than a dedicated sensor offers several advantages. First, the entire process includes both temperature and light measurements, which can be seamlessly handled by a single commercial RFID reader, eliminating the need for battery replacement or additional hardware maintenance. Second, the per-unit cost of an RFID tag is extremely low ($0.02), making this solution economically viable for large-scale or cost-sensitive applications.

While straightforward in principle, this method suffers from large pre-calibration overhead. In what follows, we propose a zero-shot calibration localization method that obtains α and β without requiring any temperature-dependent and tag-specific calibration. Such a method must eliminate the overhead of multiple light intensity measurements per tag while compensating for environmental and hardware variations dynamically.

3.4 Calibration-free Localization

Our zero-shot calibration method dynamically determines tag parameters α and β using minimal measurements from known-position light sources, eliminating the need for exhaustive manual calibration. The core insight leverages two key principles. (1) Differential measurement: By toggling a light source and measuring persistence times in "on" and "off" states, we isolate αP_{light} without prior knowledge of β or ambient conditions. (2) Invariant intensity ratios: For incoherent light sources, intensity ratios remain invariant under parameter miscalibration, enabling distance ratio estimation and tag localization. This approach not only calibrates α and β but also concurrently estimates tag positions, turning calibration into a dual-purpose process.

(1) Determining β via Light Source Switching. We propose a calibration-free approach that eliminates β through differential measurements under switched lighting conditions. Let T_{off} denote the persistence time measured in complete darkness ($P_{\text{light}} = 0$; the case of $P_{\text{light}} \neq 0$ will be discussed in Sec. 3.5). Under this condition, Eq. (4) reduces to:

$$\frac{1}{T_{\text{off}}} = \beta, \tag{6}$$

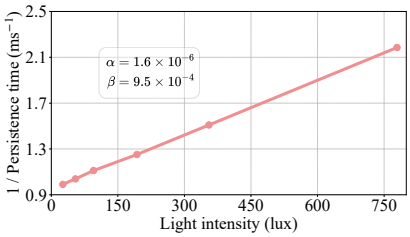

Figure 6: Linear relationship between $\frac{1}{T}$ and P_{light}.

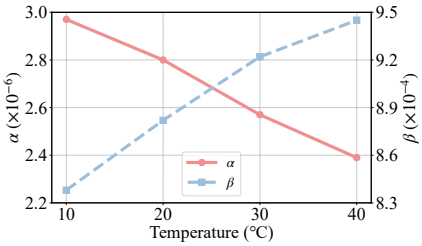

Figure 7: Influence of temperature.

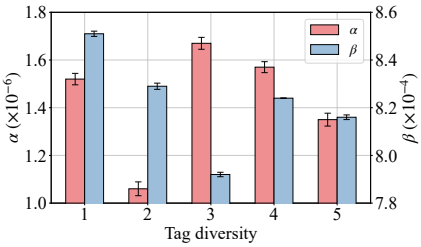

Figure 8: Influence of tag diversity.

which directly gives the value of β. When a light source is turned on, the corresponding persistence time T_{on} is measured. This yields:

$$\frac{1}{T_{\text{on}}} = \alpha P_{\text{light}} + \beta. \tag{7}$$

Since β has already been determined by Eq. (6), we can substitute it into Eq. (7) to obtain:

$$\alpha P_{\text{light}} = \frac{1}{T_{\text{on}}} - \frac{1}{T_{\text{off}}}. \tag{8}$$

The differential term $\frac{1}{T_{\text{on}}} - \frac{1}{T_{\text{off}}}$ eliminates β from the calibration process. If α is known, the current illuminance P_{light} can be computed, and vice versa.

(2) Determining α and Tag Location via Multiple Light Sources. While the differential measurement method yields β, determining α requires knowledge of P_{light}, which depends on the unknown tag-to-source distance. To address this, we leverage multiple light sources at known positions. Our key insight is that illuminance ratios remain invariant under miscalibration of α. For example, if true illuminance values are 200 lux and 400 lux, an incorrect α might report them as 150 lux and 300 lux, but their ratio (1:2) remains unchanged. This invariance stems from the linear proportionality between photocurrent I_{light} and illuminance.

Combining this with the inverse-square law ($P \propto 1/d^2$), we derive distance ratios $d_1 : d_2$ from illuminance ratios $P_1 : P_2$. For two light sources, this defines an Apollonius circle [32] of possible tag locations. With three or more sources, the intersection of these circles uniquely determines the tag's position. Once the location is known, absolute distances $d_1, d_2, \ldots$ are computed, enabling accurate calculation of P_{light} via the inverse-square law. Substituting P_{light} into Eq. (8) then gives α. This approach simultaneously resolves α and localizes the tag, turning calibration into a positioning problem without additional overhead.

More specifically, for two light sources S_1 and S_2, we have:

$$\begin{cases} \alpha P_1 = \dfrac{1}{T_{\text{on},1}} - \dfrac{1}{T_{\text{off}}}, \\ \alpha P_2 = \dfrac{1}{T_{\text{on},2}} - \dfrac{1}{T_{\text{off}}}. \end{cases} \tag{9}$$

Taking the ratio cancels α:

$$\frac{P_1}{P_2} = \frac{\frac{1}{T_{\text{on},1}} - \frac{1}{T_{\text{off}}}}{\frac{1}{T_{\text{on},2}} - \frac{1}{T_{\text{off}}}}. \tag{10}$$

For a point source radiating equally in all directions, the light intensity follows the inverse-square law:

$$P = \frac{A}{4\pi d^2}, \tag{11}$$

where d is the tag-to-source distance and A represents the radiant intensity, a constant specific to the light source. According to Eq. (10) and Eq. (11), $P_1/P_2 = d_2^2/d_1^2$, which gives the distance ratio d_1/d_2.

$$\frac{d_1}{d_2} = \sqrt{\frac{A_1}{A_2}\frac{P_2}{P_1}} = \sqrt{\frac{A_1}{A_2}\frac{\frac{1}{T_{\text{on},2}} - \frac{1}{T_{\text{off}}}}{\frac{1}{T_{\text{on},1}} - \frac{1}{T_{\text{off}}}}}, \tag{12}$$

where A_1 and A_2 are the transmit powers of the two light sources. If the two light sources have the same power, the distance ratio d_1/d_2 can be further reduced to:

$$\frac{d_1}{d_2} = \sqrt{\frac{\frac{1}{T_{\text{on},2}} - \frac{1}{T_{\text{off}}}}{\frac{1}{T_{\text{on},1}} - \frac{1}{T_{\text{off}}}}}. \tag{13}$$

Given the coordinates of two light sources: $A(x_1, y_1)$ and $B(x_2, y_2)$, and tag $C(x, y)$ with distance ratio $\frac{d_1}{d_2} = k$, where $d_1 = \|C - A\|$, $d_2 = \|C - B\|$, we have:

$$\frac{\sqrt{(x - x_1)^2 + (y - y_1)^2}}{\sqrt{(x - x_2)^2 + (y - y_2)^2}} = k. \tag{14}$$

After rearranging terms, the equation becomes the standard form of a circle:

$$x^2 + y^2 + Dx + Ey + F = 0, \tag{15}$$

where:

$$\begin{cases} D = \dfrac{-2(x_1 - k^2 x_2)}{1 - k^2}, \\ E = \dfrac{-2(y_1 - k^2 y_2)}{1 - k^2}, \\ F = \dfrac{x_1^2 + y_1^2 - k^2 x_2^2 - k^2 y_2^2}{1 - k^2}. \end{cases} \tag{16}$$

The equation satisfies the conditions for a circle because coefficients of x^2 and y^2 are equal ($= 1 - k^2$) and there is no xy cross-term. Thus, the locus of tag $C(x, y)$ is a circle, known as an Apollonius circle. This ratio defines an Apollonius circle of possible tag locations. With three or more light sources, the intersection of these circles

yields the exact tag position. Once the location is known, P_{light} is computed for each source, and α is derived via:

$$\alpha = \frac{1}{P_{\text{light}}} \left(\frac{1}{T_{\text{on}}} - \frac{1}{T_{\text{off}}} \right). \tag{17}$$

This approach offers three key benefits: (1) Minimal overhead, requiring only some persistence time measurements (dark and illuminated) through standard RFID air interface commands, eliminating the need for physical tag manipulation or dedicated hardware; (2) ambient light resilience, where subtracting on/off measurements cancels out constant ambient light interference (see Sec. 3.5); and (3) temperature independence, as both T_{on} and T_{off} are measured under identical thermal conditions, inherently compensating for temperature-induced variations in β. These features collectively enable robust, efficient calibration without environmental constraints or complex instrumentation. We stress that "zero-calibration" in this context refers specifically to the absence of pre-deployment characterization of light source properties or explicit temperature modeling, while still requiring some steps that involves toggling lights and collecting the lights' positions.

3.5 Localization under Ambient Light

Ranging and tag localization can be achieved even under ambient light conditions using the method introduced for determining α. Crucially, this process does not require total darkness ($P_{\text{env}} = 0$) to estimate β. Under ambient light ($P_{\text{env}} > 0$), toggling a light source yields:

$$\begin{cases} \frac{1}{T_{\text{off}}} = \alpha P_{\text{env}} + \beta \\ \frac{1}{T_{\text{on}}} = \alpha (P_{\text{env}} + P_{\text{light}}) + \beta. \end{cases} \tag{18}$$

Subtracting these equations eliminates αP_{env} and β:

$$\alpha P_{\text{light}} = \frac{1}{T_{\text{on}}} - \frac{1}{T_{\text{off}}}, \tag{19}$$

which is identical to the dark-condition formulation Eq. (8). This simplicity arises from the incoherence of ambient light sources. Unlike RF waves, where phase differences ($\Delta\phi$) cause constructive or destructive interference (e.g., $P_{\text{total}} = P_A + P_B + 2\sqrt{P_A P_B}\cos(\Delta\phi)$), incoherent light exhibits random phase fluctuations that average to zero over time. Thus, intensities add linearly: $P_{\text{total}} \approx P_A + P_B$. This enables direct isolation of P_{light} via subtraction, regardless of ambient conditions. Using this invariant differential measurement, we derive distance ratios $d_1 : d_2$ from illuminance ratios $P_1 : P_2$ via the inverse-square law. With four light sources, the intersection of Apollonius circles uniquely determines the tag's position, concurrently enabling calibration of α and localization without dark-environment constraints. This robustness to ambient light ensures practical deployment in real-world settings with environmental illumination.

The differential measurement removes the large calibration overhead, but it needs to toggle individual light sources, which may be infeasible in some deployments. To address this, we extend LuxTag with a complementary fingerprint-based localization mode that operates without any light control. The fingerprinting method consists of two phases. In the offline phase, the system constructs a fingerprint database by placing reference tags at known calibration points. For each point, the system records a fingerprint P_{light}, which is the light intensity derived from the tag's persistence time. During the online phase, a target tag measures its own fingerprint vector, which is then compared (e.g., via k-Nearest Neighbors) to the fingerprint database to estimate its position. This fingerprinting approach requires neither knowledge of light source positions nor the ability to toggle lights. This extension demonstrates the versatility of the persistence-time light sensing primitive. The system can be deployed in either a high-precision, controlled mode (using differential measurement with toggled lights) or a flexible, uncontrolled mode (using fingerprinting), depending on the infrastructure constraints of the target environment.

4 Implementation

In this section, we detail the implementation of LuxTag, focusing on three critical components: (1) the precise measurement of tag persistence time via RFID reader commands, (2) techniques to expand angular and range limits using optical films and lenses, and (3) the selection criteria for light sources optimized for tag responsivity and environmental compatibility.

4.1 Measurement of Persistence Time

As aforementioned, the persistence time of an RFID tag, defined as the duration the tag remains operational after RF power is removed, is a critical parameter that LuxTag exploits for ambient light sensing. This measurement is achieved by modeling the tag as an RC circuit, where the internal storage capacitor discharges once the reader's RF field is turned off. The key innovation lies in leveraging the tag's volatile memory, specifically the inventoried flag specified in the EPC Gen2 protocol [1]. By setting this flag to state 'B' during RF excitation and monitoring when it resets to 'A' during discharge, the system can precisely determine the persistence time. The process involves three phases: charging the tag's capacitor, allowing controlled discharge, and verifying functionality through Gen2 Query. This method provides high accuracy while requiring no hardware modifications, making it practical for real-world deployment. More details can be seen in [6].

To scale the measurement for multiple tags, LuxTag employs a parallelized approach that significantly reduces time overhead. Instead of testing tags individually, the system initializes all target tags simultaneously using batched Select commands, then monitors their discharge characteristics collectively. This optimization reduces measurement time by up to 90% for typical tag populations. The technique also accounts for environmental variables such as temperature, which affects leakage current and discharge rates, through differential measurements between adjacent tags. By combining these methods, LuxTag achieves robust persistence time characterization that forms the foundation for its light-based sensing and localization capabilities, all while using standard, commercial RFID hardware.

4.2 Expanding Angular and Range Limits

The tag's light sensitivity exhibits directional dependence, achieving accurate measurements when light strikes at near-perpendicular angles (incident angle $\gamma \approx 0°$). For oblique incidence ($\gamma > 0$), the effective light-receiving area decreases according to Lambert's cosine

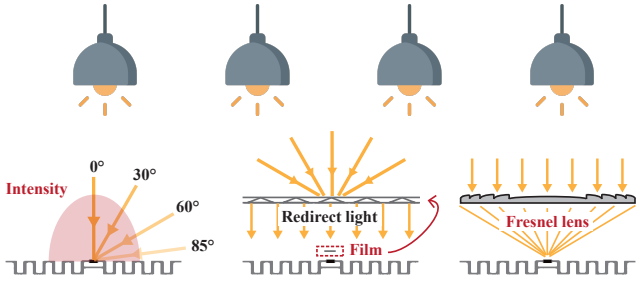

(a) Original Tag (b) Tag with a film (c) Tag with a lens

Figure 9: Expanding angular and range limits.

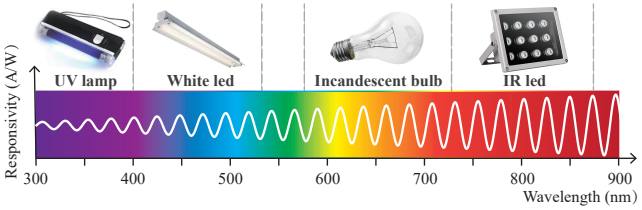

Figure 10: Tag's sensitivity to four light sources.

law, resulting in measured power:

$$P_{\text{tag}} = P_{\text{light}} \cdot \cos\gamma. \tag{20}$$

To reliably assess light intensity at a point in space (regardless of the tag's orientation), we need to mitigate this angular dependency. In this paper, we propose two complementary solutions. (1) Position-aware compensation: If the tag and light source positions are known (e.g., in positioning tasks), γ can be calculated to adjust the reading. (2) Light enhancement film: For stand-alone light sensing (as in this work), we attach a specialized film to the tag surface. As shown in Fig. 9(b), this film uses micro-prism arrays to redirect high-angle incident light ($\gamma > 60°$) toward the normal direction ($\gamma \approx 0°$), mimicking ideal cosine response. Our experiments show this extends accurate measurements to ±40°, vastly reducing orientation constraints. More evaluation details can be seen shortly later in Sec. 5.

For low-power light sources or scenarios requiring wide coverage, we boost detection range by adding a lens to concentrate light onto the tag. A conventional convex lens amplifies intensity at the tag according to:

$$P_{\text{tag}} = \left[\frac{f^2}{(f-d)^2}\right] \times P_{\text{light}}, \tag{21}$$

where f is the lens's focal length and d is the tag-to-lens distance. However, bulky convex lenses (typically > 5 mm thick) are impractical for compact deployments. Instead, we adopt a Fresnel lens (Fig. 9(c)), which compresses the optical profile of a convex lens into a flat, ultra-thin plate (~0.5 mm thick). This design dramatically expands the tag's effective sensing radius with minimal added bulk. For example, a Fresnel lens boosts the illuminance by 2.2× at the tag side. More evaluation details can be seen in Sec. 5.

4.3 Light Source

The photoelectric sensitivity of RFID tags is fundamentally determined by the semiconductor material properties of their integrated circuits. As shown in Fig. 10, through systematic testing with four distinct light sources: a 300 nm Ultraviolet (UV) lamp (commonly used for disinfection, 400-500 nm fluorescent light (cool white light), >600 nm incandescent bulb (primarily yellow/red light with some infrared), and 900 nm infrared light (IR) illuminator, we observed a clear wavelength-dependent pattern in persistence time modulation. Tags show negligible response to white LED or UV and fluorescent sources but demonstrate strong sensitivity to incandescent and IR illumination. This pattern arises because the photon-induced leakage effect occurs when photon energy exceeds the bandgap of silicon (1.1 eV, corresponding to wavelengths shorter than 1100 nm), but is most pronounced in the near-infrared (NIR) to IR range (800–1000 nm) where silicon absorption remains high and ambient noise is lower. Based on this, light sources in the 850-950 nm NIR band are optimal for LuxTag, offering three advantages: (1) alignment with silicon's peak responsivity, giving strong modulation; (2) immunity to interference from most artificial lighting; and (3) better penetration through plastics and fabrics. Two practical options are IR LEDs (efficient, directional) and incandescent bulbs (broad NIR-rich spectrum). In contrast, common phosphor-coated white LEDs, which emit primarily in the visible band with minimal NIR output, are unsuitable for LuxTag, as they induce only a weak photoelectric response in silicon-based RFID tags.

4.4 RF Interference

LuxTag's persistence-time measurement exhibits strong resilience to RF interference. We clarify this from two perspectives. In the charging phase, the Low-Dropout (LDO) regulator in the tag's power management unit ensures that the storage capacitor charges to a fixed, stable voltage before the measurement begins. This regulated charging eliminates dependence on received RF power level, distance from the reader, or the presence of ambient RF signals during the charging phase. Consequently, the capacitor's initial voltage at the start of discharge is consistent across different environments and interference conditions. In the discharging phase, our measurement protocol operates within Session S1 in EPC Gen2, where inventory commands (e.g., Query, QueryRep) do not recharge the tag [6]. This allows the tag to discharge freely while being repeatedly inventoried, isolating the discharge process from additional RF energy. Therefore, during the discharge window, the tag is not being actively powered by the reader or by ambient interference in a way that would alter its discharge dynamics.

4.5 Deployment Comparison

LuxTag's deployment consists of three key components: a standard EPC Gen2 RFID reader with a single antenna, multiple light sources (e.g., incandescent bulbs or IR LEDs), and battery-free passive tags. The reader and antenna are positioned to cover the target area, while light sources are strategically placed to ensure adequate illumination overlap. Notably, LuxTag requires no specialized

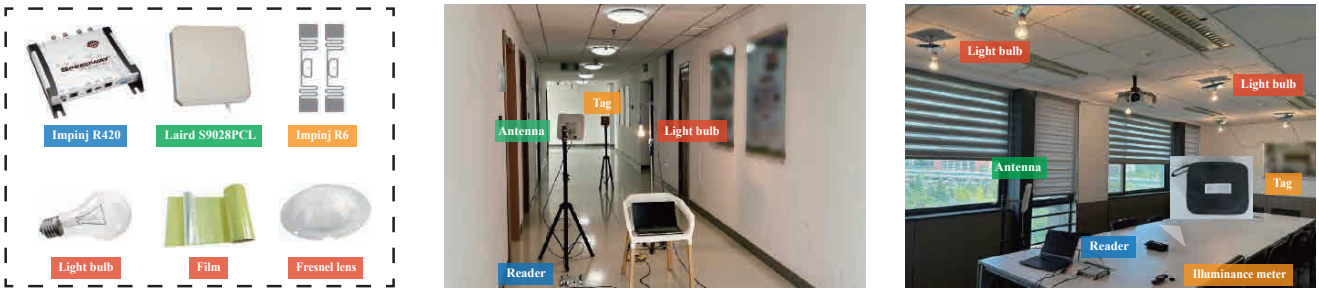

(a) Devices (b) Corridor (c) Office

Figure 11: System setup.

hardware modifications: all components are commercial off-the-shelf. The light sources operate on standard power circuits without needing synchronization or modulation, significantly reducing infrastructure complexity compared to specialized RF-based systems. Existing static RFID localization approaches face greater deployment cost. Trilateralion methods [14, 34] typically require multiple reader/antennas precisely positioned around the perimeter, with careful cable management and phase synchronization. Angle-of-Arrival (AoA) systems [16, 28] demand expensive antenna arrays with precise geometric calibration and specialized signal processing hardware. Both approaches necessitate extensive site surveys and higher hardware cost, comparison to LuxTag.

5 Evaluation

In this section, we set up the LuxTag system and evaluate its performance, in terms of the accuracy of light sensing, the impact of environmental factors, the ranging accuracy, and the accuracy of static localization.

5.1 Evaluation Setup

In our experiments, we deploy an Impinj R420 reader [11] connected to a TE S9028 antenna [23] to measure the persistence time of RFID tags. The tag model used in the experiment is the Impinj R6P (ER62) [11], which serves as LuxTag devices. A DLY-1802 luminance meter is used as the ground truth reference. A host laptop (Intel Core i7-14650HX, 5.2 GHz, 16 GB RAM) controlled the reader via Java-based software implementing the EPC Gen2 Low-Level Reader Protocol (LLRP) for standardized communication. We use the absolute error between the estimated value and the ground truth as the performance metric, defined as the 'Estimation Error'. Two real-world scenarios (corridor and office room) are tested for light sensing, ranging, and localization.

Light Source. To identify optimal illuminants for LuxTag, we measured the persistence time of an Impinj R6 tag at distances of 0.5 m and 1.0 m under four light sources: a 300 nm UV lamp, a 400-500 nm white LED, a >600 nm incandescent bulb, and a 900 nm IR LED. As shown in Fig. 12, IR-rich sources (incandescent and IR LED) produce strong persistence-time modulation, decreasing by 35% and 31%, respectively, when the distance is halved. In contrast, UV and white-LED sources induce negligible change (<1%) because their spectra fall outside the silicon IC's high-responsivity band. These results confirm that LuxTag performs best with IR-rich illumination; we therefore use an incandescent bulb as the default source in all following experiments.

5.2 Accuracy of Illuminance Sensing

We begin by evaluating the performance of LuxTag for illuminance sensing. The experimental setup is illustrated in Fig. 11(b). An incandescent bulb is used to control the light intensity incident on the tag. To establish the baseline, we first use a luminance meter at various distances (e.g., 1 m, 2 m, 3 m) from the bulb to model its radiation pattern and determine parameter A in Eq. (11). The tag and the bulb are typically placed at the same height; however, it is important to note that LuxTag does not require such alignment in practical light sensing applications. This controlled setup is primarily adopted to ensure the accuracy of the ground-truth illuminance values derived from Eq. (11).

Sensing Accuracy: In the first experiment, we study the accuracy of LuxTag when sensing the illuminance, where the tag-to-source distances (light intensities) range from 1.5 m to 4 m. To derive the parameter α, we utilize the calibrated radiation model of the bulb to calculate its light intensity (P_{light}) at 1 m. Then, we measure the persistence time (T_{on} and T_{off}) by switching the bulb. Substituting these three parameters into Eq. (17) allows us to derive α. Using α together with T_{on} and T_{off} measured at other locations and substituting into Eq. (8), we can determine the current illumination intensity, which will be used to compute the accuracy. As shown in Fig. 13, the mean measurement errors of LuxTag are 4.6 lux, 3.35 lux, 3 lux, 3.11 lux, 4.7 lux, 6.19 lux, at the six testing distances respectively. The positive results reveal that LuxTag achieves remarkable illuminance sensing accuracy across varying distances while demonstrating predictable performance characteristics. More specifically, the system maintains stable illuminance estimation errors between 3-4 lux at distances ranging from 1.5 to 3 meters, indicating robust performance within this operational range. This consistency demonstrates the effectiveness of our persistence time-based sensing model under typical deployment conditions. Beyond 3 meters, we observe a gradual increase in estimation error, reaching approximately 6.2 lux at 4 meters.

Taking a deeper look at the sensing accuracy, we also plot the cumulative distribution function (CDF) of measurement errors across

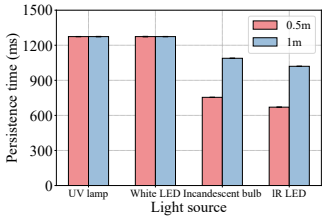

Figure 12: Impact of light source.

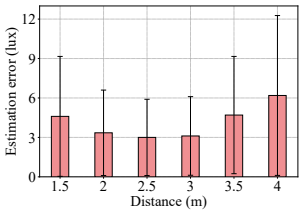

Figure 13: Illuminance sensing accuracy.

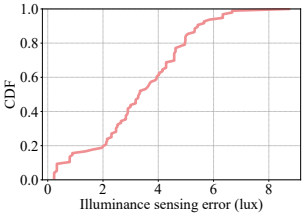

Figure 14: CDF of measurement error.

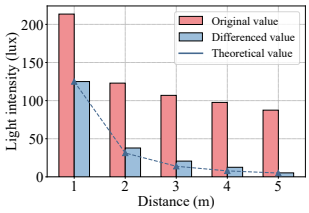

Figure 15: Impact of ambient light.

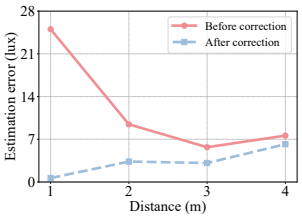

Figure 16: Impact of temperature.

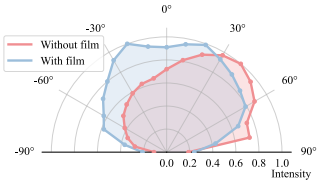

Figure 17: Impact of tag orientation.

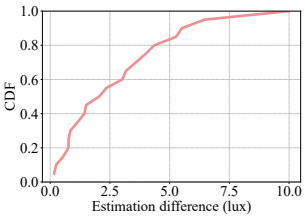

Figure 18: Impact of tag diversity.

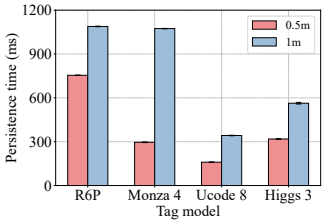

Figure 19: Impact of tag model.

all distances. As shown in Fig. 14, the 50% of the measurement errors are bounded within 3.3 lux, while 90% of the measurement errors are within 6.3 lux. This confirms LuxTag's practical viability for real-world deployment, sufficient for centimeter-level positioning accuracy when combined with our localization algorithm.

Impact of ambient light: A critical capability in tag-based localization is accurately measuring the illumination from a specific light source. To achieve this, we introduce a differential measurement approach: the light bulb is switched on and off sequentially, and the difference between the two readings is used to isolate the target source's contribution. We evaluate the method under realistic conditions, including strong ambient sunlight. If the measured values are accurate enough for distance estimation, the extracted light intensity should follow the theoretical inverse-square law, i.e., when the distance doubles, the intensity should drop to one quarter of its original value. The results are summarized in Fig. 15. As shown, the differential measurements (blue bars) correspond closely to the theoretical curve. At 1 meter, the measured intensity is 124.9 lux. At 2 meters, the theoretical value is 31.2 lux, while our measurement yields 37.8 lux, a deviation of only 6.6 lux. In contrast, the raw measurement under sunlight (red bar) is 122.9 lux, which is clearly unsuitable for ranging due to strong ambient interference. This experiment confirms the effectiveness of our approach in suppressing environmental light.

Impact of temperature: Temperature has a significant impact on persistence time, which represents a core challenge for the practical application of our method. Below, we compare the performance of using fixed parameters versus computed parameters under varying thermal conditions. In the experiment, we first calibrate the parameters at $0°C$ and then use them to estimate the light intensity at $30°C$. As shown in Fig. 16, this approach introduce a maximum error of 25 lux at 1 meter. Overall, the error decreased as the light intensity diminished. When the intensity approached zero, the measurement error become comparable to that obtained with correct parameters, though a slight increase occurred due to diffuse reflection. We also derive the parameters through calibration at 1 meter and applied them to measurements taken at 2, 3, and 4 meters. The results show that the errors are all bounded within 7 lux, significantly reducing the measurement errors caused by temperature variation.

Impact of tag orientation: The relative angle between the tag and the light source plays a critical role in its light capture capability. LuxTag using a brightness-enhancing film on the tag to enhance the measurement. In the experiment, we rotate a tag for $-90°$ to $+90°$ and measure the corresponding illuminance. After deriving all measurements, we compute the ratio of the measured value to the maximum measured value. As we can see in Fig. 17, with cosine correction (brightness-enhancing film), LuxTag achieves a $100°$ angular range within which it can stably measure up to 80% of the maximum light intensity. Without the film, the tag's measurements are highly sensitive to angle variations, with the peak value occurring at around $+40°$. The angular range of 80% is only $50°$. LuxTag achieves 2× performance gains.

Impact of tag diversity: We then study the impact of tag diversity. In the experiment, we first calibrate the tag parameters at a distance of 1 meter, and then used these registered parameters to measure the light intensity from 1 to 4 meters. In Fig. 18, we plot the cumulative distribution function (CDF) of the differences between the measurements from the 5 tags across various distances. The results show strong agreement between the 5 tags under the same conditions: the average difference in measured light intensity is 2.85 lux, and the median error is 2.20 lux. Given a reference value of 125 lux at 1 meter, a deviation of 2.2 lux corresponds to a spatial error of only 0.88 cm. These results indicate that the inter-tag variation in light measurement is negligible.

Impact of tag model: To verify the generality of the photoelectric effect, we test four COTS tag models: Impinj R6 [13], Impinj Monza 4 [12], NXP UCODE 8 [20], and Alien Higgs 3 [3]. Each

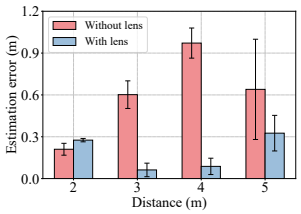

Figure 20: Ranging accuracy.

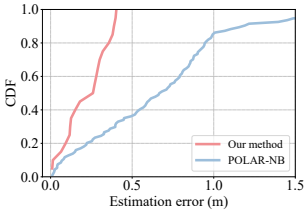

Figure 21: Localization accuracy.

tag is exposed to an incandescent bulb at two distances. As shown in Fig. 19, all models exhibit a consistent, significant reduction in persistence time under stronger illumination. While absolute persistence times varied due to differences in internal capacitance and baseline leakage, the relative change remained substantial and measurable for every tag model. This confirms that the photon-induced leakage current (a fundamental property of the silicon PN junctions used in passive RFID ICs) is universally present across commercial designs, establishing LuxTag's broad compatibility with off-the-shelf hardware.

5.3 Ranging & Localization Accuracy

We next study the ranging and localization accuracy. As shown in Fig. 11(c), six light bulbs with known positions are mounted on the ceiling. During the experiment, LuxTag is used to measure distances or distance ratios to enable conventional triangulation-based localization. We then present the performance of our system for both single-bulb distance measurement and multi-bulb localization scenarios.

LuxTag-based ranging: We first evaluate the ranging accuracy of our system. After calibrating a tag to determine its parameters, we estimate the distance between the tag and a light source across a range of distances from 2 to 5 meters. As shown in Fig. 20, LuxTag achieves high ranging accuracy with a mean error of 18.7 cm when enhanced with an optical lens. This lens significantly amplifies received light intensity, enabling reliable distance estimation even at larger distances. In contrast, the tag without a lens receives insufficient light, resulting in poor ranging performance due to inadequate signal strength.

LuxTag-based localization: We next compare our system with POLAR-NB [7], the state-of-the-art static RFID localization method based on ToF using narrowband signals. The CDF of localization errors (Fig. 21) demonstrates that LuxTag significantly outperforms POLAR-NB under the C1G2 standard, which strictly limits available bandwidth. LuxTag achieves a mean error of 22.5 cm, a substantial improvement over POLAR-NB's 57 cm. This enhancement stems from LuxTag's inherent robustness to multipath interference by leveraging optical sensing principles immune to RF-specific artifacts. Notably, while POLAR-NB could achieve higher accuracy with larger bandwidth, such configurations violate C1G2 compliance and are impractical for commercial RFID deployments. LuxTag thus provides a standards-compliant, high-accuracy solution for static tag localization. Note that while methods like Tagoram [34] and RF-Chord [16] represent significant advances in RFID localization, they are not suitable as direct baselines for our work due to fundamental incompatibilities with our problem setting. Tagoram relies on tag movement to resolve phase ambiguities (i.e., the 0-2π jumps in phase measurements) through synthetic aperture radar techniques; however, it fails to use fixed reader to localize static tags because the phase information remains ambiguous without spatial diversity. In contrast, LuxTag targets static tag localization, where both tags and infrastructure are fixed. On the other hand, RF-Chord utilizes a wide bandwidth (up to 200 MHz) for time-of-flight (TOF) measurements, which theoretically supports static tag localization. Yet, this approach violates the FCC regulations for commercial UHF RFID systems, which are limited to a narrow bandwidth of 28 MHz. Consequently, RF-Chord is incompatible with standard COTS RFID hardware and cannot be deployed in practical scenarios. Given that POLAR-NB operates under the same narrowband constraints as LuxTag and addresses static localization within C1G2 standards, it serves as the most appropriate and fair baseline for comparison. This choice ensures that our evaluation reflects real-world deployability and highlights LuxTag's advantages under standardized conditions.

6 Related Work

RFID localization provides unparalleled advantages for item-level tracking in indoor environments, offering inherent identification capabilities and battery-free operation that traditional wireless systems like WiFi and bluetooth cannot match. Traditional RFID localization primarily leverages RF signal properties such as Received Signal Strength Indicator (RSSI) [14, 22], phase difference [16, 28, 34], or Doppler shift [2, 24]. While these methods have achieved notable progress, they fundamentally struggle with non-line-of-sight (NLOS) conditions and multipath propagation – an enduring problem in RF systems [8, 18, 27]. These multipath effects arise from the specular (mirror-like) reflection behavior of RF waves, where wavelengths (e.g., $\lambda \approx 0.3$ m for UHF RFID) are often significantly larger than the average surface roughness at common environmental boundaries like walls or shelving units. Consequently, signals reflect coherently, leading to complex superposition at the receiver that is exceptionally difficult to model or disentangle, particularly for narrow-band RFID systems.

To address these issues, in recent years, Synthetic Aperture Radar (SAR) techniques [4, 26, 29, 34] have been adopted to enhance spatial resolution by synthesizing a virtual antenna array through controlled reader movement. These methods fundamentally rely on capturing RSSI or phase measurements from multiple spatial positions along the reader's trajectory. By analyzing the RSSI or phase difference between these positions, they achieve precise position estimation. Some advanced work has been developed in the last decade. Yang et al. [34] propose a Differential Augmented Hologram (DAH) algorithm to achieve millimeter-level accuracy by virtually synthesizing an antenna array from tag motion. Bernardini et al. [4] propose a robot-assisted SAR method for UHF-RFID tag localization, using multiple trajectories to enhance spatial diversity and improve accuracy in complex indoor settings. Tripicchio et al. [26] develop a synthetic aperture UHF-RFID technique combining phase unwrapping and hyperbolic intersection to resolve phase ambiguities and achieve precise tag positioning. Nevertheless, these methods demand not only specialized hardware, precise motion

control, and extensive environmental profiling, but also inherently rely on dynamic spatial sampling to construct a continuous phase profile—a condition fundamentally absent in static deployments, where tags and infrastructure remain stationary.

Accurate and scalable static RFID localization remains an open problem in real-world settings. Recent attempts have drawn inspiration from Ultra-Wideband (UWB) systems by employing Time-of-Flight (ToF) measurements in RFID systems [17]. These efforts aim to achieve decimeter-level accuracy by estimating signal propagation time through direct path propagation time measurement. Subsequent work incorporate polarization diversity to reduce orientation-dependent errors [7]. However, a fundamental limitation arises from the spectral regulations imposed by the FCC: commercial UHF RFID systems are restricted to narrowband operation (e.g., 902–928 MHz with limited channel bandwidth), whereas UWB requires several gigahertz of bandwidth for high time-resolution. This bandwidth constraint severely limits temporal resolution, with state-of-the-art systems achieving median localization errors of approximately 57 cm [7] – insufficient for applications requiring higher accuracy.

In contrast to RF-based methods, our work LuxTag introduces a paradigm shift by leveraging optical signals to overcome multipath and bandwidth limitations. The core advantage of LuxTag lies in its ability to perform accurate localization under a fully static infrastructure, where both the RFID reader and all tags remain completely stationary. This stands in direct opposition to SAR-based methods that require controlled movement to resolve spatial ambiguities. By exploiting the persistence time of COTS RFID tags as a proxy for ambient light intensity, we enable accurate ranging immune to RF-specific artifacts. Our approach requires no hardware modifications, operates within FCC-mandated narrow bands, and achieves a low localization error of 22.5 cm, all while maintaining full compatibility with existing RFID infrastructure. This capability to deliver high precision without any dependency on motion makes LuxTag uniquely suited for real-world deployments where tags are fixed and reader movement is impractical. This fusion of optical sensing and RF communication bridges a critical gap in scalable, high-accuracy RFID localization for static scenarios.

Compared to traditional ambient light localization systems [10, 15, 35, 36], LuxTag also offers distinct advantages: (1) Battery-free operation using standard RFID tags eliminates power constraints and hardware costs; (2) compatibility with ambient light sources (e.g., IR LEDs, incandescent bulbs) minimizes infrastructure requirements; (3) preservation of native RFID identification capabilities enables simultaneous ID resolution and precision localization without additional instrumentation. This unique combination of battery-free operation, minimal infrastructure requirements, and dual-purpose identification/localization distinguishes LuxTag from prior ambient light systems and underscores its practical utility in real-world deployments.

7 Conclusion, Limitation, Future Work

This paper has introduced LuxTag, a novel system that enables accurate, low-cost light-based localization using standard commercial off-the-shelf (COTS) passive RFID tags. By exploiting the discovery that ambient light modulates a tag's persistence time, we transformed standard passive tags into optical sensors without hardware modifications. The core innovation lies in modeling the photon-induced leakage current in tag circuitry, which accelerates capacitor discharge proportionally to illuminance, and establishing the inverse-linear relationship between persistence time and illuminance. We further propose a zero-shot calibration method that dynamically determines system parameters using differential measurements, eliminating the need for laborious per-tag or temperature-dependent manual calibration. This method not only enables robust calibration under ambient light but also concurrently estimates tag positions through multi-source triangulation based on invariant illuminance ratios, effectively turning calibration into a dual-purpose localization process. LuxTag bridges the gap between RF infrastructure and optical sensing, combining the deployment simplicity and ubiquity of RFID with the multipath resilience of light-based ranging. This work opens new avenues for low-cost, high-precision indoor localization in applications such as warehouses, smart factories, and retail environments.

While LuxTag demonstrates high accuracy in controlled environments, its real-world deployment faces inherent challenges and opens avenues for broader application. A fundamental limitation of LuxTag, and all optical systems, is its reliance on a direct line-of-sight (LOS) between the light source and the tag. This restricts its use to open environments like warehouses with open shelving or retail spaces with well-placed lighting. A promising direction to overcome this limitation is the development of a hybrid RF-light localization framework, wherein ubiquitous yet coarse-grained RF measurements (e.g., RSSI or phase) provide continuous tracking and coarse position estimation for non-LOS tags, while LuxTag's high-precision light-based ranging serves as a correction or refinement layer. We emphasize that LuxTag is not intended to replace existing RF-based localization methods but rather to complement and enhance them, offering an alternative and highly accurate solution for static RFID localization in suitable deployment scenarios.

Another exciting and natural extension of LuxTag is its potential for optical communication. Our method demonstrates that a standard RFID tag can be used as a crude but functional light intensity sensor. This capability can be repurposed to receive data by modulating a light source. The primary challenge lies in the low data rate constrained by the relatively slow discharge and measurement cycle of persistence time. Future research will focus on optimizing the modulation scheme and developing novel, higher-speed methods to measure the photocurrent's effect, potentially pushing data rates into the tens or hundreds of bits per second, sufficient for many practical command-and-control applications.

Acknowledgments

This work was supported in part by the China Postdoctoral Science Foundation (GZB20240306), Natural Science Foundation of Jiangsu Province (BK20241247), Jing-Jin-Ji Regional Integrated Environmental Improvement-National Science and Technology Major Project (2025ZD1208203), Jiangsu Funding Program for Excellent Postdoctoral Talent (2024ZB504), Collaborative Innovation Center of Novel Software Technology and Industrialization, and Fundamental and Interdisciplinary Disciplines Breakthrough Plan of the Ministry of Education of China (JYB2025XDXM118).

References

[1] 2024. *GS1 EPCglobal. EPC radio-frequency identity protocols generation-2 UHF RFID version 3.0.*

[2] Abeer Ahmad, Yuanfei Huang, Xiao Sha, Akshay Athalye, Milutin Stanaćević, Samir R Das, and Petar M Djurić. 2020. On measuring doppler shifts between tags in a backscattering tag-to-tag network with applications in tracking. In *ICASSP 2020-2020 IEEE International Conference on Acoustics, Speech and Signal Processing (ICASSP)*. IEEE, 9055–9059.

[3] Alien. 2026. Alien Higgs 3. *https://www.alientechnology.com/products/ic/higgs-3/* (2026).

[4] Fabio Bernardini, Alice Buffi, Daniele Fontanelli, David Macii, Valerio Magnago, Mirko Marracci, Andrea Motroni, Paolo Nepa, and Bernardo Tellini. 2020. Robot-based indoor positioning of UHF-RFID tags: The SAR method with multiple trajectories. *IEEE Transactions on Instrumentation and Measurement* 70 (2020), 1–15.

[5] Xingyu Chen, Jia Liu, Xia Wang, Haisong Liu, Dong Jiang, and Lijun Chen. 2020. Eingerprint: Robust energy-related fingerprinting for passive RFID tags. In *Proc. of USENIX NSDI*. 1101–1113.

[6] Xingyu Chen, Jia Liu, Fu Xiao, Shigang Chen, and Lijun Chen. 2021. Thermotag: Item-level temperature sensing with a passive RFID tag. In *Proc. of ACM MobiSys*. 163–174.

[7] Laura Dodds, Isaac Perper, Aline Eid, and Fadel Adib. 2023. A handheld fine-grained rfid localization system with complex-controlled polarization. In *Proc. of ACM MobiCom*. 1–15.

[8] Xiaoyi Fan, Feng Wang, Wei Gong, Lei Zhang, and Jiangchuan Liu. 2018. Multiple object activity identification using RFIDs: A multipath-aware deep learning solution. In *Proc. of IEEE ICDCS)*. 545–555.

[9] Chao Feng, Jie Xiong, Liqiong Chang, Fuwei Wang, Ju Wang, and Dingyi Fang. 2021. RF-identity: Non-intrusive person identification based on commodity RFID devices. *Proceedings of the ACM on Interactive, Mobile, Wearable and Ubiquitous Technologies* 5, 1 (2021), 1–23.

[10] Chenting Gu, Xiaofeng Liu, Yongsheng Ou, Chao Liu, Hao Tao, and Tianyun Shi. 2020. Led visible light localization based on illuminance analysis. In *Proc. of IEEE RCAR*. 393–398.

[11] Impinj. 2025. Impinj Inc. http://www.impinj.com.

[12] Impinj. 2026. Impinj Monza 4. *https://support.impinj.com/hc/en-us/articles/202756908-Monza-4-Datasheet* (2026).

[13] Impinj. 2026. Impinj R6P. *https://support.impinj.com/hc/en-us/articles/204793258-Monza-R6-P-Product-Brief-Datasheet* (2026).

[14] Chenglong Li, Emmeric Tanghe, David Plets, Pieter Suanet, Jeroen Hoebeke, Eli De Poorter, and Wout Joseph. 2020. ReLoc: Hybrid RSSI-and phase-based relative UHF-RFID tag localization with COTS devices. *IEEE Transactions on Instrumentation and Measurement* 69, 10 (2020), 8613–8627.

[15] Lingkun Li, Pengjin Xie, and Jiliang Wang. 2018. Rainbowlight: Towards low cost ambient light positioning with mobile phones. In *Proc. of ACM MobiCom*. 445–457.

[16] Bo Liang, Purui Wang, Renjie Zhao, Heyu Guo, Pengyu Zhang, Junchen Guo, Shunmin Zhu, Hongqiang Harry Liu, Xinyu Zhang, and Chenren Xu. 2023. RF-Chord: Towards deployable RFID localization system for logistic networks. In *Proc. of USENIX NSDI*. 1783–1799.

[17] Yunfei Ma, Nicholas Selby, and Fadel Adib. 2017. Minding the billions: Ultra-wideband localization for deployed RFID tags. In *Proc. of ACM MobiCom*. 248–260.

[18] Martin Maderböck and Thomas Ussmueller. 2023. Multicarrier communication for UHF RFID: Increased reliability and coverage for uhf RFID systems. *IEEE Microwave Magazine* 24, 10 (2023), 51–58.

[19] John Nolan, Kun Qian, and Xinyu Zhang. 2024. Keystub: A passive rfid-based keypad interface using resonant stubs. *Proceedings of the ACM on Interactive, Mobile, Wearable and Ubiquitous Technologies* 7, 4 (2024), 1–23.

[20] NXP. 2026. NXP UCODE 8. *https://www.nxp.com/products/SL3S1205-15* (2026).

[21] Longfei Shangguan and Kyle Jamieson. 2016. The design and implementation of a mobile RFID tag sorting robot. In *Proceedings of the 14th annual international conference on mobile systems, applications, and services*. 31–42.

[22] Saurav Subedi, Eric Pauls, and Yimin D Zhang. 2017. Accurate localization and tracking of a passive RFID reader based on RSSI measurements. *IEEE Journal of Radio Frequency Identification* 1, 2 (2017), 144–154.

[23] TE. 2025. TE CONNECTIVITY. https://www.te.com/.

[24] Deivid A Tesch, Everton L Berz, and Fabiano P Hessel. 2015. RFID indoor localization based on Doppler effect. In *Sixteenth international symposium on quality electronic design*. IEEE, 556–560.

[25] Shuai Tong, Zhenqiang Xu, and Jiliang Wang. 2020. Colora: Enabling multi-packet reception in lora. In *Proc. of IEEE INFOCOM*. 2303–2311.

[26] Paolo Tripicchio, Matteo Unetti, Salvatore D'Avella, Alice Buffi, Andrea Motroni, Fabio Bernardini, and Paolo Nepa. 2021. A synthetic aperture UHF RFID localization method by phase unwrapping and hyperbolic intersection. *IEEE Transactions on Automation Science and Engineering* 19, 2 (2021), 933–945.

[27] Ge Wang, Xiaofeng Shi, Haofan Cai, Chen Qian, Han Ding, Wei Xi, Kun Zhao, Jizhong Zhao, and Jinsong Han. 2022. A Generalized method to combat multipaths for RFID sensing. *IEEE/ACM Transactions on Networking* 31, 1 (2022), 336–351.

[28] Ju Wang, Jie Xiong, Hongbo Jiang, Xiaojiang Chen, and Dingyi Fang. 2016. D-watch: Embracing "bad" multipaths for device-free localization with COTS RFID devices. In *Proc. of ACM CoNEXT*. 253–266.

[29] Xianping Wang, Daniele Inserra, Guangjun Wen, and Paolo Nepa. 2024. A Synthetic Aperture Radar UHF RFID Localization Method Based on Phase Jumps. In *2024 IEEE 12th Asia-Pacific Conference on Antennas and Propagation (APCAP)*. IEEE, 1–2.

[30] Yanwen Wang and Yuanqing Zheng. 2018. Modeling RFID signal reflection for contact-free activity recognition. *Proceedings of the ACM on Interactive, Mobile, Wearable and Ubiquitous Technologies* 2, 4 (2018), 1–22.

[31] Ziyi Wang, Yihong Chen, Hao Zheng, Meng Liu, and Ping Huang. 2023. Body RFID skeleton-based human activity recognition using graph convolution neural network. *IEEE Transactions on Mobile Computing* 23, 6 (2023), 7301–7317.

[32] wolfram mathworld. 2025. Apollonian circles. https://mathworld.wolfram.com/ApolloniusCircle.html.

[33] Weiye Xu, Jianwei Liu, Shimin Zhang, Yuanqing Zheng, Feng Lin, Jinsong Han, Fu Xiao, and Kui Ren. 2021. RFace: Anti-spoofing facial authentication using COTS RFID. In *Proc. of IEEE INFOCOM*. 1–10.

[34] Lei Yang, Yekui Chen, Xiang-Yang Li, Chaowei Xiao, Mo Li, and Yunhao Liu. 2014. Tagoram: real-time tracking of mobile RFID tags to high precision using COTS devices.. In *MobiCom*, Vol. 10. 2639108–2639111.

[35] Lin Yang, Zeyu Wang, Wei Wang, and Qian Zhang. 2018. NALoc: Nonlinear ambient-light-sensor-based localization system. *Proceedings of the ACM on Interactive, Mobile, Wearable and Ubiquitous Technologies* 2, 4 (2018), 1–22.

[36] Yuanpeng Zhang, Xiansheng Yang, Xiao Sun, Yaxin Wang, Tianbing Ma, and Yuan Zhuang. 2023. Diffuse reflection effects in visible light positioning: analysis, modeling, and evaluation. *Electronics* 12, 17 (2023), 3646.

[37] Yuanqing Zheng and Mo Li. 2013. ZOE: Fast cardinality estimation for large-scale RFID systems. In *2013 Proceedings IEEE INFOCOM*. IEEE, 908–916.

[38] Sisi Zhou and Liang Jiang. 2019. Modern description of Rayleigh's criterion. *Physical Review A* 99, 1 (2019), 013808.

[39] Yuan Zhuang, Luchi Hua, Longning Qi, Jun Yang, Pan Cao, Yue Cao, Yongpeng Wu, John Thompson, and Harald Haas. 2018. A survey of positioning systems using visible LED lights. *IEEE Communications Surveys & Tutorials* 20, 3 (2018), 1963–1988.